nature geoscience

LETTERS

PUBLISHED ONLINE: 21 OCTOBER 2012 | DOI: 10.1038/NGEO1610

The 2011 Lorca earthquake slip distribution controlled by groundwater crustal unloading

Pablo J. González[1]*, Kristy F. Tiampo[1], Mimmo Palano[2], Flavio Cannavó[2] and José Fernández[3]

Earthquake initiation, propagation and arrest are influenced by fault frictional properties[1,2] and preseismic stress[3,4]. Studies of triggered and induced seismicity[5–7] can provide unique insights into this influence. However, measurements of near-field, surface ground deformation[8,9] and pre-earthquake stress conditions necessary for such studies are rare. Here, we use geodetic data to determine surface deformation associated with the M_w 5.1 earthquake that occurred in Lorca, southeast Spain, on 11 May 2011. We use an elastic dislocation model to show that earthquake nucleation and the area of main fault slip occurred at very shallow depths of 2–4 km, on a rupture plane along the Alhama de Murcia Fault. Slip extended towards the surface, across fault segments with frictional properties that changed from unstable to stable. The area of fault slip correlates well with the pattern of positive Coulomb stress change that we calculate to result from the extraction of groundwater in a nearby basin aquifer. We therefore suggest that the distribution of shallow slip during the Lorca earthquake could be controlled by crustal unloading stresses at the upper frictional transition of the seismogenic layer, induced by groundwater extraction. Our results imply that anthropogenic activities could influence how and when earthquakes occur.

The Eastern Betics Shear Zone in southeastern Spain is a transpressive deformation segment of the major diffuse Nubia–Eurasia plate boundary (Fig. 1a), where an approximately northwest–southeast convergence motion is accommodated in a complex set of thrusting and strike-slip faults[10,11]. This region has suffered a significant number of moderate-to-large earthquakes in the past 500 years and is considered one of the areas of highest seismic risk in Spain[12]. On 11 May 2011 (16:47 UTC), an earthquake struck the city of Lorca (Fig. 1b), causing significant property damage, injuring hundreds and resulting in nine fatalities. The epicentre, as determined by the National Geographical Institute of Spain (IGN), was located ~2 km east-northeast of Lorca, with a focal mechanism solution indicative of reverse and strike-slip faulting that occurred at very shallow crustal depths (~3 km; ref. 12). The mainshock has been tentatively attributed to a major fault in the area, the Alhama de Murcia Fault[12] (AMF). Catalogue locations for the entire sequence (~149 events) present an undistinguished pattern[12]; however, detailed seismic relocation indicates that most events were generated along the AMF (ref. 13; Fig. 1b).

To constrain the coseismic slip, surface deformation was measured by radar interferometry. In addition, available GPS (global positioning system) data were processed both at daily and at 1 Hz rates to determine static and transient offsets (see Methods). Two different ENVISAT descending satellite tracks (I2 and I6) imaged the area before and after the event, providing estimates of the displacement field from two different look angles (Fig. 2a,c). Differential interferograms were processed in time series without temporal filtering (see Methods) and resulting displacement maps were corrected for a known groundwater subsidence signal[14] (Fig. 1c,d and Supplementary Information). Coseismic displacement maps show displacements towards the satellite north of the mapped AMF (ref. 11), with deformation peaks at ~2.5 cm (Fig. 2a) and ~1.5 cm (Fig. 2c). Deformation reversed south of the AMF, with ~1 cm of displacement away from the satellite (Fig. 2a,c). Finally, deformations in the urban area and southeastwards with respect to the AMF branch show maximum displacements. All the continuous GPS stations except LORC were stable (Figs 1a and 2a,c). LORC station moved north (4.2 ± 0.8 mm) and slightly to the west (-0.9 ± 0.8 mm), although the vertical motion was not significant. Postseismic deformation can be considered negligible, as evidenced by the absence of transients in the following hours to days at LORC (see Supplementary Information).

We model the ground deformation data using an elastic dislocation model[15]. First, we explored for the nonlinear dislocation geometry[16], and then solved for the distributed slip. The best-fitting uniform dislocation model indicates a reverse and left-lateral slip fault striking N230 E and dipping 70° to the northeast at very shallow depths (1 ± 0.3 km to 4 ± 0.8 km down dip). These parameters indicate that the earthquake rupture occurred along the AMF, and the results are in good agreement with seismically derived focal parameters[12]. However, large residuals are found near downtown Lorca (see Supplementary Information). The fault slip distribution was resolved on an extended fault plane (10×10 km^2) with a slightly modified strike to match the asymmetric pattern observed in the interferograms (N225 E). The preferred smoothed distributed fault slip model allows for two patches of relative maximum slip. A slip area with mainly oblique motion (reverse and left-lateral, ~15 cm) occurs beneath the La Tercia segment-AMF north of the city of Lorca, at depths ranging from 2 to 5 km, which is consistent with an independent fault slip model estimated using a TerraSAR-X differential interferogram[17]. A much shallower and smaller slip area with left-lateral to pure reverse motion is found beneath the city along the Lorca segment-AMF, ~5 cm (Fig. 3a). According to the surface geology, the AMF southeastern branch has been identified as a vertical or south-dipping thrust, from Totana (~15 km northeast) to Lorca[11,18]. If a small vertical segment (down to 1 km) is introduced in the fault geometry the data fit is improved

[1]Department of Earth Sciences, University of Western Ontario, Biological and Geological Sciences Building, London, Ontario N6A 5B7, Canada, [2]Istituto Nazionale di Geofisica e Vulcanologia, Osservatorio Etneo—Sezione di Catania, Piazza Roma 2, 95123 Catania, Italy, [3]Instituto de Geociencias (CSIC-UCM), Facultad de Ciencias Matemáticas, Plaza de Ciencias 3, Ciudad Universitaria, 28040 Madrid, Spain. *e-mail: pgonzal4@uwo.ca.

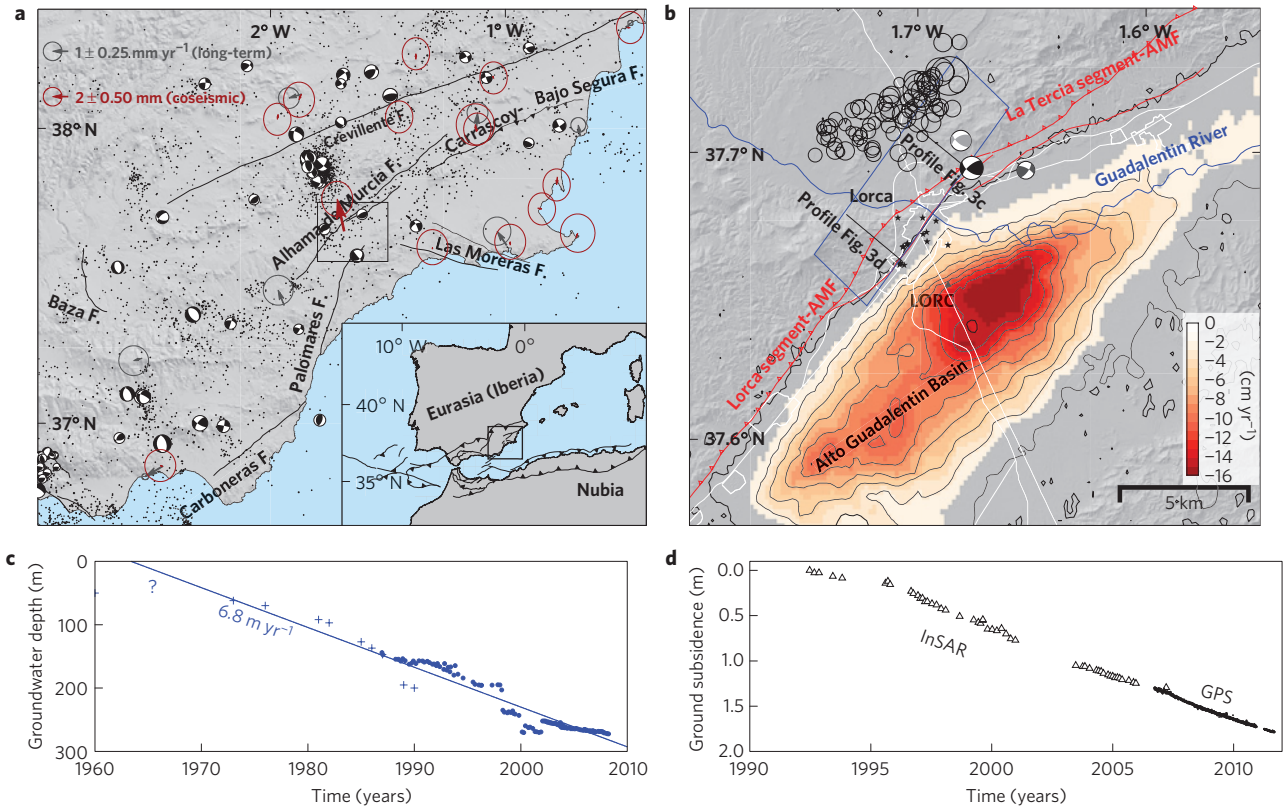

Figure 1 | Location and kinematics of the Lorca earthquake. a, Southwest Spain seismicity (2000–2010), focal mechanisms (1970–2010), long-term GPS velocity (2006–2011, grey) and coseismic vectors (red). Major mapped faults are labelled. **b**, Lorca city and Alto Guadalentin Basin. IGN mainshock focal mechanisms (black), pre-shock (light grey) and largest aftershock (dark grey), and relocated seismic sequence[13]. The black stars are damage locations; the red lines are faults[11]. The contour lines indicate 2 cm yr^{-1} InSAR subsidence due to groundwater pumping[14]. Blue rectangle: fault surface projection. AMF, Alhama de Murcia Fault. **c**, Groundwater depth evolution from different data sources (see Supplementary Information). **d**, InSAR (triangles) and line-of-sight (LOS)-projected GPS ground-surface subsidence at LORC station.

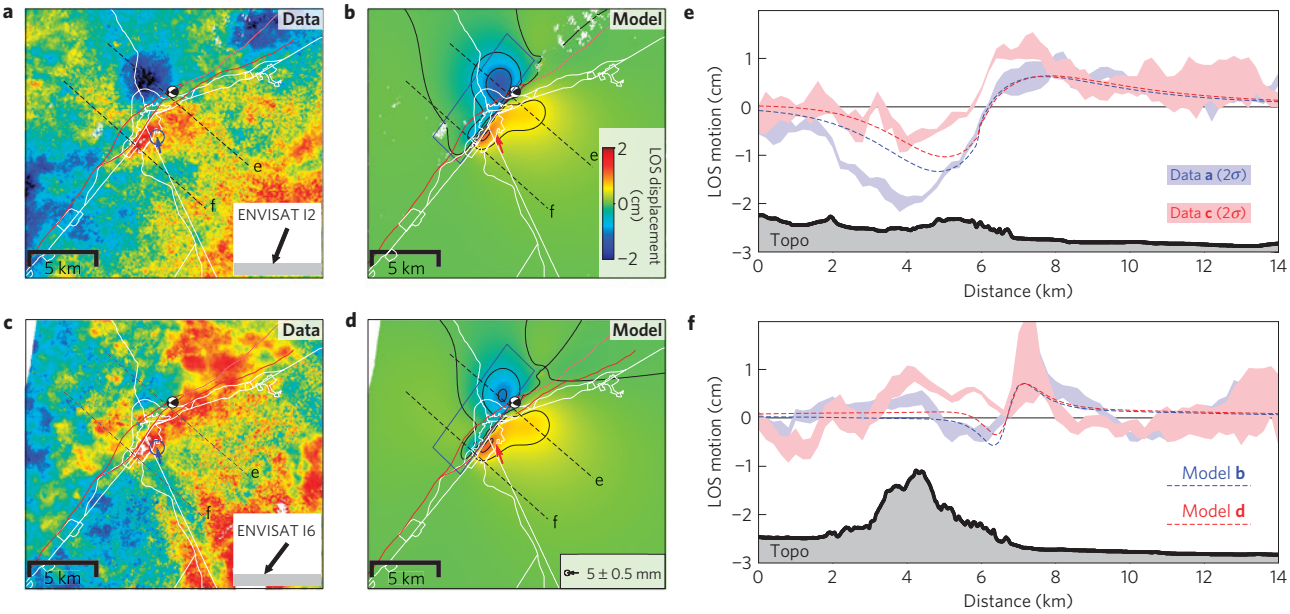

Figure 2 | Ground deformation data and model. a–**d**, Descending LOS displacement maps and LORC station horizontal GPS vector (**a** and **c**) and distributed slip model predictions (**b** and **d**). **a**,**b**, Data and model for track 008 (20110426–20110526). **c**,**d**, Data and model for track 209 (20110510–20110609). The insets in **a** and **c** indicate LOS angle, positive values away from the satellite. Blue rectangle: fault surface projection. Dashed lines are profile locations (**a**–**d**). **e**,**f**, Observed and simulated data along two profiles, and local topography. 2σ data profiles based on standard deviation in a 1-km-wide area normal to the profile direction.

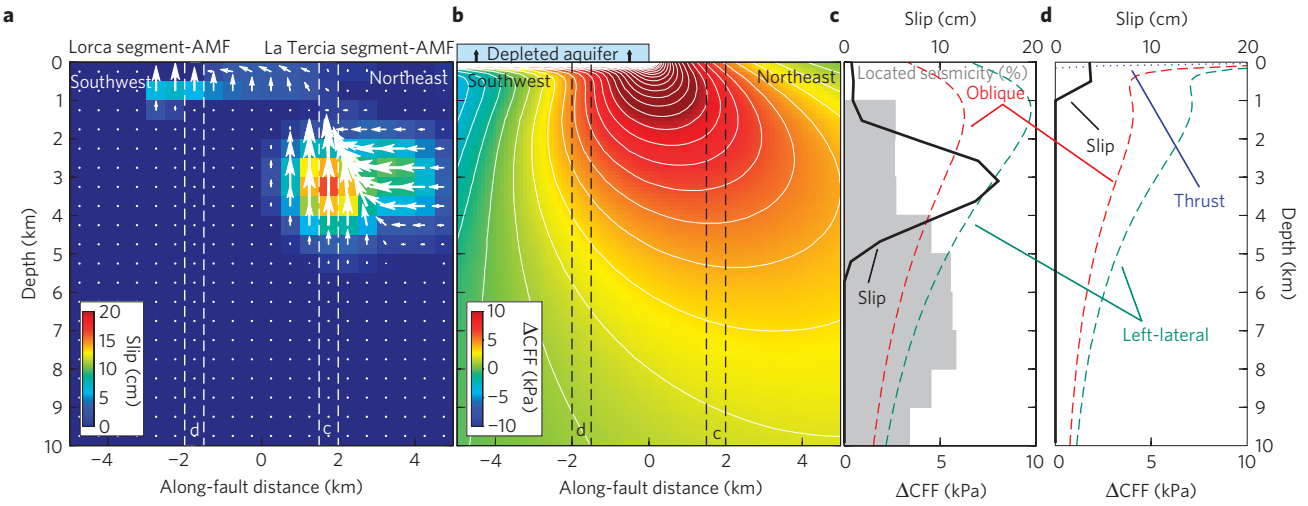

Figure 3 | Fault slip and unloading stress change models. a, Coseismic distributed fault slip model. **b**, Fifty years (~1960–2010) of cumulative ΔCFF (slip rake = 36°) resolved on the rupture fault plane by crustal unloading. **c**,**d**, Fault dip profiles ~2.5 km north of the city (**c**) and in Lorca (**d**) for the coseismic slip, and three cumulative unloading ΔCFF models with variable slip rake (thrusting,blue; left-lateral, green; oblique, red with rake = 36°). The background of **c** shows the depth percentage of the long-term crustal seismicity (2000–2010) located (www.ign.es) in southwest Spain, under a similar compressive regime, used to infer the depth of the upper frictional transition limit.

(Fig. 2b,d). However, this does not significantly modify the slip pattern (see Supplementary Information).

Crustal (un-)loading due to near-surface mass redistribution (water, ice or quarried material) can affect the subsurface stress field altering magma production[19] and seismic activity[20–22]. The Alto Guadalentin Basin shows high subsidence rates, >10 cm yr^{-1}, due to long-term sustained groundwater pumping[14] (Fig. 1d). The subsidence area is bounded by nearby faults (for example, AMF) and the Guadalentin River (Fig. 1b), indicative of possible permeability barriers or structural control in the deposition of compressible sediments. Regional groundwater depletion and related environmental problems have been recognized since the 1960s (ref. 23). Although groundwater table level changes are available only at a few wells, Fig. 1c shows groundwater depth evolution between ~1960 and 2010, which indicates a drop of at least 250 m. We investigate whether or not the groundwater extraction activity could significantly affect the tectonic fault that was activated during the Lorca earthquake, as the unusual shallow slip may indicate. Here, we calculate the three-dimensional subsurface stress change induced by the crustal load on a homogeneous elastic half-space using the Boussinesq solution[24] and resolve for the Coulomb stress change (ΔCFF) on the fault geometry. We explored a range of possible (unknown) groundwater-table-change areal shapes, aquifer porosities, the role of pore-pressure diffusion, and fault friction (see Supplementary Information). In Fig. 3b, we present ΔCFF resolved along the AMF with a slip rake of 36°, in accordance with the published focal mechanisms. We assume conservative values for the unloading model parameters and a simple aquifer shape based on the aquifer permeability barriers, as these provide a lower bound model for the possible stress changes due to the pumping and permanent groundwater drawdown[23] (see Supplementary Information).

The actual interseismic slip rate and stress/friction conditions on the fault are unknown, which precludes their specific inclusion in the stress model. However, before the 2011 earthquake, the most recent similar, moderate earthquake on the AMF near Lorca occurred in 1818 (ref. 12). From palaeoseismic estimates for net fault slip (0.07–0.6 mm yr^{-1}; ref. 11), the accumulated slip deficit ranges from 1.4 to 12 cm. The upper bound is in good agreement with the estimated maximum coseismic slip magnitude for this event, indicating that the fault had accumulated sufficient interseismic tectonic stress to allow for a similar earthquake rupture, assuming that it had remained fully locked.

Given that the faulting itself was tectonically driven, the pattern of unloading stress changes due to the anthropogenic groundwater changes coincides to a remarkable degree with the areas of significant coseismic slip (Fig. 3a,b). Assuming that the hypocentral location coincides with rupture nucleation, slip begins north and outwards of the unloaded aquifer area with a left-lateral to reverse slip component. Consistently, we find maximum values of ΔCFF (Fig. 3c) for left-lateral to oblique slip motions; such higher values are due to the relative increase of shear stress change at this region. The ΔCFF model also favours propagation towards the surface laterally along the fault-bounded aquifer as thrust rupture. All studied models predict an increase in ΔCFF towards the surface. This propagation pattern also is supported by analysis of radiated seismic energy directivities[13,25], which are consistent with a predominantly southwest and towards-the-surface rupture. However, ΔCFF decreases to smaller values for left-lateral slip rake beneath the unloading and far from the aquifer border (Fig. 3b), whereas thrust motion increases owing to shallow induced extension (reduction of normal stresses) at depths of 1 km or less (Fig. 3d). Conversely, the unloading model also explains the slip arrest, as the slip turns and is dominated by a reverse slip component southwest of the city (Fig. 3a). Slip propagation ultimately is limited by the Earth surface boundary and the low values of pre-stress for encouraging left-lateral rupture motion along a parallel outward-dipping fault at the same location (Fig. 3). The arrest of the coseismic slip propagation in this location also coincides with the intense shaking and damage in the southwestern part of Lorca (Barrio de La Viña).

On the basis of established studies of fault mechanics[26], depth-dependent fault frictional change and reduced stresses close to the surface prevent surface coseismic slip[2,5]. These limit the maximum slip area during seismic rupture, inferred from geodetic and seismic data to occur at middle crustal depths of 3–8 km (ref. 5). The inferred slip depth here may indicate that the rupture nucleated at the transition zone between velocity-weakening and velocity-strengthening zones (Fig. 3c). The fault slip propagation towards the surface and into the velocity-strengthening area would require that anomalously high dynamic stresses develop at the

crack tip and/or a thick fault gouge[26]. Although the shallow slip area could be an early afterslip effect, it would be limited to the first 15 days following the earthquake, in accordance with the radar data (Fig. 2a,c). Again, LORC GPS station shows no evidence of postseismic motion. We favour shallow coseismic slip on the basis of the interpretation that the high-stress conditions required to propagate coseismic slip into the shallow velocity-strengthening volume were probably in place before the event, as a consequence of the cumulative long-term unloading stress change and the relative position of the fault with respect to the depleted aquifer (mainly shallow extension parallel to the unloading source and left-lateral shear at the aquifer edge boundary). It has been shown that three-dimensional crustal (un-)loading processes can promote long-term fault slip or modulate seismicity beneath the (un-)loading source[20,27,28] and on the periphery[22,29]. Here we present observations and modelling results for a possible link between the crustal unloading and the slip pattern during a single earthquake.

We conclude that the presented data and modelling results are consistent with a groundwater crustal unloading process, providing a reasonable explanation for the observed fault slip pattern, as well the propagation and arrest of fault slip during the earthquake into the shallow crustal velocity-strengthening fault zone. This study reveals an unexpected human-induced alteration of the ambient subsurface stress field close to an active seismogenic source, and provides insights into processes that could modify the seismic hazard in this region and elsewhere.

Methods

We correct the differential interferograms for orbital trends by adjusting a bilinear function in a least-squares sense. We estimated the bilinear model using the entire interferogram. Masking the deformation area has a negligible effect. We estimated for the displacement time series and associated errors using a multi-temporal InSAR time-series method (see Supplementary Information). It takes into account decorrelation, individual atmospheric noise, and observation redundancy from a Monte Carlo estimation process[30]. Interferogram atmospheric noise was estimated by fitting a one-dimensional zero-order Bessel and exponential covariance function based on randomly distributed points, but excluding points in the deformation region. The final displacement maps were obtained by differencing the time series, and errors for each coherent pixel ($\rho > 0.2$) in the displacement map were obtained by error propagation of estimated formal errors for each considered time series step.

GPS data were analysed using all continuous stations in southwest Spain spanning the 2006.00–2011.67 period (dates given in decimal years). The processing of GPS data was done using two different strategies. All data sets were processed on a daily basis by using the GAMIT-GLOBK software packages to characterize the long-term and coseismic deformation patterns (Fig. 1). A three-day period of high-rate data (1 Hz sampling) was processed by applying the instantaneous GPS positioning method to detect transient deformation associated with the earthquake occurrence (see Supplementary Information).

In the unloading mechanical model, we assumed 50 years (~1960–2010) of cumulative ΔCFF (slip rake $= 36°$) resolved on the rupture fault plane by crustal unloading due to 5 m yr^{-1} of groundwater table drop in an aquifer with 5% effective porosity. We approximate the aquifer shape as a rectangular unloading source shape (10×8 km^2 area, shown in Supplementary Fig. S11a). The vertex of the aquifer is coincident with the point where the mapped fault trace changes in strike (La Tercia and Lorca segments of AMF), north of Lorca. At this location, the aquifer- and mapped groundwater-induced subsidence areas are limited by the Guadalentin River, which runs approximately perpendicular to the Lorca-AMF segment (Fig. 1b and Supplementary Fig. S11a). We assumed values for fault friction, $c = 0.5$, and Skempton coefficient, $B = 0.6$. Other models were also tested (see Supplementary Information). Files containing the displacement maps, fault slip distribution model and location of point sources for loading modelling can be obtained on request to the corresponding author.

Received 10 January 2012; accepted 20 September 2012; published online 21 October 2012

References

1. Dieterich, J. H. Modeling of rock friction: 1. Experimental results and constitutive equations. *J. Geophys. Res.* **84,** 2161–2168 (1979).
2. Marone, C. & Scholz, C. H. The depth of seismic faulting and the upper transition from stable to unstable slip regimes. *Geophys. Res. Lett.* **15,** 621–624 (1988).
3. Kaneko, Y., Avouac, J-P. & Lapusta, N. Towards inferring earthquake patterns from geodetic observations of interseismic coupling. *Nature Geosci.* **3,** 365–369 (2010).
4. Loveless, J. P. & Meade, B. J. Spatial correlation of interseismic coupling and coseismic rupture extent of the 2011 Mw = 9.0 Tohoku-oki earthquake. *Geophys. Res. Lett.* **38,** L17306 (2011).
5. Simpson, D. W. Triggered earthquakes. *Annu. Rev. Earth Planet Sci.* **14,** 21–42 (1986).
6. Seeber, L., Armbruster, J. G., Kim, W-Y., Barstow, N. & Scharnberger, C. The 1994 Cacoosing Valley earthquakes near Reading, Pennsylvania: A shallow rupture triggered by quarry unloading. *J. Geophys. Res.* **103,** 24505–24521 (1998).
7. McCarr, A., Simpson, D. & Seeber, L. in *International Handbook of Earthquake and Engineering Seismology* vol. 81A (eds Lee, W. H. K., Kanamori, H., Jennings, P. C. & Kisslinger, C.) (Academic, 2002).
8. Fialko, Y., Sandwell, D., Simons, M. & Rosen, P. Three-dimensional deformation caused by the Bam, Iran, earthquake and the origin of shallow slip deficit. *Nature* **435,** 295–299 (2005).
9. Fielding, E. J., Lundgren, P. L., Bürgmann, R. & Funning, G. J. Shallow fault-zone dilatancy recovery after the 2003 Bam earthquake in Iran. *Nature* **458,** 64–68 (2009).
10. Stich, D., Serpelloni, E., Mancilla, F. & Morales, J. Kinematics of the Iberia-Maghreb plate contact from seismic moment tensors and GPS observations. *Tectonophysics* **426,** 295–317 (2006).
11. Masana, E., Martínez-Díaz, J. J., Hernández-Enrile, J. L. & Santanach, P. The Alhama de Murcia fault (southwest Spain), a seismogenic fault in a diffuse plate boundary: Seismotectonic implications for the Ibero-Magrebian region. *J. Geophys. Res.* **109,** B01301 (2004).
12. IGN, Informe del sismo de Lorca del 11 de Mayo de 2011 [in Spanish] (http://www.ign.es/ign/resources/sismologia/Lorca.pdf, 2011).
13. Lopez-Comino, J. A., Mancilla, F. d. L., Morales, J. & Stich, D. Rupture directivity of the 2011, Mw 5.2 Lorca earthquake (Spain). *Geophys. Res. Lett.* **39,** L03301 (2012).
14. González, P. J. & Fernández, J. Drought-driven transient aquifer compaction imaged using multitemporal satellite radar interferometry. *Geology* **39,** 551–554 (2011).
15. Okada, Y. Surface deformation due to shear and tensile faults in a half-space. *Bull. Seismol. Soc. Am.* **75,** 1135–1154 (1985).
16. González, P. J., Tiampo, K. F., Camacho, A. G. & Fernández, J. Shallow flank deformation at Cumbre Vieja volcano (Canary Islands): Implications on the stability of steep-sided volcano flanks at oceanic islands. *Earth Planet. Sci. Lett.* **297,** 545–557 (2010).
17. Frontera, T. *et al.* DInSAR coseismic deformation of the May 2011 Mw 5.1 Lorca earthquake (southeastern Spain). *Solid Earth* **3,** 111–119 (2012).
18. Martínez-Díaz, J. J. Stress field variations related to fault interaction in a reverse oblique-slip fault: The Alhama de Murcia fault, Betic Cordillera, Spain. *Tectonophysics* **356,** 291–305 (2002).
19. Hooper, A. *et al.* Increased capture of magma in the crust promoted by ice-cap retreat in Iceland. *Nature Geosci.* **4,** 783–786 (2011).
20. Heki, K. Snow load and seasonal variation of earthquake occurrence in Japan. *Earth Planet. Sci. Lett.* **207,** 159–164 (2003).
21. Klose, C. D. Geomechanical modeling of the nucleation process of Australia's 1989 M5.6 Newcastle earthquake. *Earth Planet. Sci. Lett.* **256,** 547–553 (2007).
22. Bettinelli, P. *et al.* Seasonal variations of seismicity and geodetic strain in the Himalaya induced by surface hydrology. *Earth Planet. Sci. Lett.* **266,** 332–344 (2008).
23. Cerón, J. C. & Pulido-Bosch, A. Groundwater problems resulting from CO_2 pollution and overexploitation in Alto Guadalentín aquifer (Murcia, Spain). *Environ. Geol.* **28,** 223–228 (1996).
24. Boussinesq, J. Application des Potentiels à l'Étude de l'Équilibre et du Mouvement des Solides Élastiques (Reprint Paris: Blanchard, 1969, (1885)).
25. Rueda, J., Mezcua, J. & Garcia Blanco, R. M. Directivity effects of the May 11, 2011 Lorca (Spain) Mw = 5.1 earthquake, S53B-2277, 2011 Fall Meeting, AGU, San Francisco, California, 5–9 Dec. (2011).
26. Marone, C., Scholz, C. & Bilham, R. On the mechanics of earthquake afterslip. *J. Geophys. Res.* **96,** 8441–8452 (1991).
27. Hetzel, R. & Hampel, A. Slip rate variations on normal faults during glacial-interglacial changes in surface loads. *Nature* **435,** 486–492 (2011).
28. Brothers, D., Kilb, D., Luttrell, K., Driscoll, N. & Kent, G. Loading of the San Andreas fault by flood-induced rupture of faults beneath the Salton Sea. *Nature Geosci.* **4,** 486–492 (2011).
29. Hampel, A., Hetzel, R., Maniatis, G. & Karow, T. Three-dimensional numerical modeling of slip rate variations on normal and thrust fault arrays during ice cap growth and melting. *J. Geophys. Res.* **114,** B08406 (2008).

30. González, P.J. & Fernández, J. Error estimation in multitemporal InSAR deformation time series, with application to Lanzarote, Canary Islands. *J. Geophys. Res.* **116,** B10404 (2011).

Acknowledgements

Our research was financially supported by an Ontario Early Researcher Award, the CSRN NSERC Strategic Network Grant, and the NSERC and Aon Benfield/ICLR IRC in Earthquake Hazard Assessment. P.J.G. also acknowledges the Banting Postdoctoral Fellowship of the Government of Canada. Further support was provided by the projects CGL2005-05500-C02, CGL2008-06426-C01-01/BTE, PCI2006-A7-0660 and AYA2010-17448; as well the Moncloa International Campus of Excellence. Radar data were from ESA CAT1:4460 and 6745 projects. GPS data were from Meristemum, Red Activa de Murcia and IGN networks. GMT software was used to create all figures. We are grateful to J-P. Avoua for helpful comments. We thank P. Bhattacharya, N. Cho and F. Lorenzo-Martín for stimulating discussions, F. Luzón, and J. Morales and A. Concha for sharing manuscripts before publication[13,17].

Author contributions

P.J.G. carried out the radar data analysis; dislocation, loading and pore-pressure diffusion models; and wrote the manuscript with the help of all co-authors. K.F.T. and P.J.G. carried out the CFF models. M.P. processed daily GPS data and computed the two-dimensional strain-rate tensor. F.C. processed high-rate GPS data and analysed accelerometer frequency spectra. J.F. and P.J.G. designed the research.

Additional information

Supplementary information is available in the online version of the paper. Reprints and permissions information is available online at www.nature.com/reprints. Correspondence and requests for materials should be addressed to P.J.G.

Competing financial interests

The authors declare no competing financial interests.